Structure of the Biliverdin Radical Intermediate in Phycocyanobilin:Ferredoxin Oxidoreductase Identified by High-Field EPR and DFT

Stefan Stoll,*,[†] Alexander Gunn,[†] Marcin Brynda,[†,||] Wesley Sughrue,[†,‡]
Amanda C. Kohler,[‡,⊥] Andrew Ozarowski,[§] Andrew J. Fisher,[†,‡] J. Clark Lagarias,[‡]
and R. David Britt*,[†]

*Department of Chemistry and Section of Molecular and Cellular Biology, University of
California Davis, 1 Shields Avenue, Davis, California 95616, and National High Magnetic Field
Laboratory, Florida State University, 1800 East Paul Dirac Drive, Tallahassee, Florida 32310*

Received October 31, 2008; E-mail: sstoll@ucdavis.edu (S.S.); rdbritt@ucdavis.edu (R.D.B.)

The cyanobacterial enzyme phycocyanobilin:ferredoxin oxidoreductase (PcyA) catalyzes the two-step four-electron reduction of biliverdin IXα to phycocyanobilin, the precursor of biliprotein chromophores found in phycobilisomes. It is known that catalysis proceeds via paramagnetic radical intermediates, but the structure of these intermediates and the transfer pathways for the four protons involved are not known. In this study, high-field electron paramagnetic resonance (EPR) spectroscopy of frozen solutions and single crystals of the one-electron reduced protein−substrate complex of two PcyA mutants D105N from the cyanobacteria *Synechocystis* sp. PCC6803 and *Nostoc* sp. PCC7120 are examined. Detailed analysis of *Synechocystis* D105N mutant spectra at 130 and 406 GHz reveals a biliverdin radical with a very narrow *g* tensor with principal values 2.00359(5), 2.00341(5), and 2.00218(5). Using density-functional theory (DFT) computations to explore the possible protonation states of the biliverdin radical, it is shown that this *g* tensor is consistent with a biliverdin radical where the carbonyl oxygen atoms on both the A and the D pyrrole rings are protonated. This experiment all confirms the reaction mechanism recently proposed (Tu, et al. *Biochemistry* **2007**, *46*, 1484).

Introduction

In cyanobacteria and red algae, phycobilisomes are light-harvesting protein complexes that absorb light and transfer the captured energy to the chlorophylls in the photosynthetic reaction centers.[1,2] The constituents of the phycobilisomes are proteins that carry chromophore cofactors covalently linked to the apoproteins via thioether linkages to cysteine residues.[3] The chromophores are open-chain tetrapyrroles known as bilins that are responsible for the strong absorption and fluorescence characteristics of the phycobiliproteins. The varied nature of the chromophores allows these organisms to capture light over a spectral range wider than that of chlorophylls and carotenoids found in higher plants. Bilins common in cyanobacteria include phycocyanobilin and phycoerythrobilin.

The common precursor in the biosynthesis of all bilins is heme, which is converted to biliverdin IXα (BV) by heme oxygenase.[4,5] From there, various specialized ferredoxin-de-
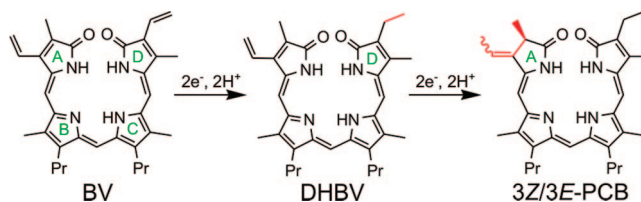
Figure 1. Two consecutive reactions catalyzed by PcyA (BV = biliverdin IXα, DHBV = $18^1,18^2$-dihydrobiliverdin, PCB = phycocyanobilin, Pr = propionate).

pendent biliverdin reductases (FDBRs) produce the chromophores by regioselective reduction of one or more double bonds.[6−8] Among these enzymes, phycocyanobilin:ferredoxin oxidoreductase (PcyA) catalyzes the synthesis of phycocyanobilin in a two-step reduction of biliverdin to 3*Z*/3*E*-phycocyanobilin (3*Z*/3*E*-PCB) via the intermediate $18^1,18^2$-dihydrobiliverdin (DHBV),[9] as illustrated in Figure 1. In the first step,

[†] Department of Chemistry.
[||] Present address: Department of Physical Chemistry, Sciences II, University of Geneva, 30 Quai Ernest Ansermet, 1211 Geneva, Switzerland.
[‡] Section of Molecular and Cellular Biology.
[⊥] Present address: The Rockefeller University, 1230 York Ave., Box 384, New York, NY 10065.
[§] National High Magnetic Field Laboratory.

(1) Glazer, A. N. *Annu. Rev. Biophys. Biophys. Chem.* **1985**, *14*, 47–77.
(2) MacColl, R. *J. Stuct. Biol.* **1998**, *124*, 311–334.
(3) Scheer, H.; Zhao, K. H. *Mol. Microbiol.* **2008**, *68*, 263–276.
(4) Beale, S. I. *Chem. Rev.* **1993**, *93*, 785–802.

(5) Frankenberg, N.; Lagarias, J. C. In *The Porphyrin Handbook*; Kadish, K. M., Smith K. M., Guilard, R., Eds.; Academic Press: San Diego, 2003; Vol. 13, p 211−235.
(6) Frankenberg, N.; Mukougawa, K.; Kohchi, T.; Lagarias, J. C. *Plant Cell* **2001**, *13*, 965–978.
(7) Dammeyer, T.; Hofmann, E.; Frankenberg-Dinkel, N. *J. Biol. Chem.* **2008**, *283*, 27547–27554.
(8) Tu, S. L.; Chen, H.-C.; Ku, L.-W. *J. Biol. Chem.* **2008**, *283*, 27555–27564.
(9) Frankenberg, N.; Lagarias, J. C. *J. Biol. Chem.* **2003**, *278*, 9219–9226.

the exovinyl group on ring D is reduced, and in the second step, the A ring with its endovinyl group is targeted.

PcyA is unusual in several ways: It catalyzes a two-step four-electron reduction instead of a one-step two-electron reduction with the two-electron reduced intermediate DHBV not being released from the enzyme. The only other four-electron bilin reductase is the recently discovered phycoerythrobilin synthase from the cyanophage PSSM-2.[7] In contrast to the NAD(P)H-dependent biliverdin reductase (BVR), which catalyzes the reduction of BV to bilirubin in mammals, PcyA uses ferredoxin (Fd) as a reducing agent. Unlike practically all other Fd-dependent enzymes, PcyA lacks other cofactors (flavins, iron−sulfur clusters, etc.) to deliver the electrons from reduced Fd to the substrate. For in vitro turnover, only BV and reduced Fd are needed.

On the basis of biochemical, UV/vis, and electron paramagnetic resonance (EPR) spectroscopic evidence, we have shown that the PcyA reaction proceeds via transient paramagnetic radical intermediates.[10] Two residues near the active site (H88 and D105, using the numbering from *Synechocystis* sp. PCC 6803) proved to be essential for catalysis.[11] In this regard, the D105N and H88Q mutants generated stable EPR-detectable radical intermediates,[11] both of which were similar to the transient radical previously observed for PcyA wild type.[10] However, neither mutant yielded significant amounts of DHBV. On the basis of this evidence and three available crystal structures,[12−14] a reaction mechanism involving proton transfers (PTs) and four electron transfer (ETs) step was proposed.[10,14] The mechanisms of these reduction steps remain undetermined. It is not known whether they proceed via stepwise ET-PT or PT-ET, or in a concerted proton-coupled electron transfer (PCET) fashion.[15] The precise structures of the paramagnetic intermediates, especially their charges and protonation states, are also unclear.

The present investigation was undertaken to determine the structure of the stable paramagnetic intermediate generated by the one-electron reduction of the D105N mutant. Here we employ EPR spectroscopy at high (4.6 T, 130 GHz) and very high fields (14.5 T, 406 GHz). High-field EPR[16,17] is a powerful technique for elucidating structures of radical intermediates in enzymatic redox reactions: since EPR spectroscopy is selective for paramagnetic species, diamagnetic enzyme−substrate and enzyme−product complexes do not interfere with these measurements. In addition, the very small anisotropy (<0.4%) of the g tensors of organic radicals that cannot be resolved in spectra obtained with conventional EPR at low fields (0.4 T, 10 GHz) can be determined by high-field EPR. Moreover, much can be learned about the electronic structure of the radical from the anisotropy of the g tensor. In this study, experimental high-field EPR data combined with evidence from X-ray crystal structures and g tensor predictions from density functional theory

(DFT) computations are used to assess the structure of the bilin radical intermediate of the D105N mutant in PcyA. From this information, we can identify the protonation state of the BV radical intermediate, providing direct spectroscopic evidence for the recently proposed reaction mechanism for bilin reduction by PcyA.

Experimental Procedures

Site-Directed Mutagenesis, Expression, and Purification of PcyA Mutants. Mutants of *Nostoc* sp. PCC7120 were generated using the expression vector pGEX-6-P1. Glutathione S-transferase-tagged PcyA mutant proteins were overexpressed in DH5α *E. coli* grown in LB medium for 6 h at 37 °C. Inductions were performed overnight at 18 °C with isopropyl thio-β-D-galactopyranoside, and cells were harvested by centrifugation followed by lysis with a Microfluidizer. Cell lysates were centrifuged at 87 000g and 4 °C for 30 min, and supernatants were applied to pre-equilibrated glutathione−agarose columns. Tagged proteins were eluted using reduced glutathione, concentrated using Amicon Ultra 10 000 MWCO concentrators, dialyzed overnight against TKG (25 mM TES-KOH at pH 8.5, 100 mM KCl, 10% glycerol), concentrated to 2 mM, as determined by BCA assay,[18] and stored at −80 °C after flash-freezing in liquid nitrogen. *Synechocystis* sp. PCC 6803 PcyA mutants were generated using the expression vector pTYB12 (New England Biolabs). Intein-tagged protein was overexpressed in BL21 *E. coli* grown in LB medium for 6 h at 37 °C. Induction was performed overnight at 12 °C with lactose, and cells were harvested by centrifugation. After lysis, cell lysate was centrifuged and supernatant was applied to a chitin column pre-equilibrated with buffer (50 mM Tris-HCl, pH 8.0, 500 mM NaCl). After subsequent washes of buffer, intein self-cleavage was induced with 100 mM dithiothreitol in buffer for 36 h. Protein was eluted with buffer and concentrated using Amicon Ultra 10,000 MWCO concentrators. Dialysis, concentration, and storage were identical to *Nostoc* proteins.

Ferredoxin. Recombinant *Synechococcus* sp. PCC7002 ferredoxin was expressed and purified as described previously.[19] Dialysis was performed against TKG (25 mM TES-KOH, pH 8.5, 100 mM KCl, 10% glycerol). The concentration was adjusted to 1 mM on the basis of absorption measurement at 420 nm (extinction coefficient 9.7 mM^{-1} cm^{-1}) and stored at −20 °C.

Biliverdin. Biliverdin IXα was prepared from commercially obtained bilirubin as described previously.[20]

Crystals. Crystals of BV bound *Synechocystis* D105N PcyA were obtained under safe green light using the hanging-drop method with a drop size of 4 μL on 24-well Linbro plates. Drops contained 2 μL of reservoir buffer plus 2 μL of PcyA-BV solution. Crystals were grown at 20 °C in the dark. These conditions produced rectangular crystals that were dark blue in their native state. Conditions that resulted in the best diffracting crystals were 1.45−1.8 M (NH$_4$)$_2$SO$_4$, 0.15−0.4 M NaCl, and 0.1 M HEPES buffer at pH 7.0. The crystals were typically 0.4 mm × 0.2 mm × 0.1 mm in size. For production of the radical intermediates, crystals were soaked in 100 mM sodium dithionite in reservoir buffer solution and allowed to sit in the dark until a color change from blue to green occurred (typically within 10 min). The reduced crystals were mounted into 0.50 mm i.d./0.60 mm o.d. quartz tubes (VitroCom, Mountain Lakes, NJ) for the 130 GHz EPR measurements and flash-frozen in liquid nitrogen. Details of the X-ray crystal structures will be published separately. The coordinates of BV and its surrounding amino acid residues in the crystal are included in the Supporting Information (Tables S1 and S2). The symmetry of the radical crystals is orthorhombic (space group

(10) Tu, S. L.; Gunn, A.; Toney, M. D.; Britt, R. D.; Lagarias, J. C. *J. Am. Chem. Soc.* **2004**, *126*, 8682–8693.

(11) Tu, S. L.; Sughrue, W.; Britt, R. D.; Lagarias, J. C. *J. Biol. Chem.* **2006**, *281*, 3127–3136.

(12) Hagiwara, Y.; Sugishima, M.; Takahashi, Y.; Fukuyama, K. *FEBS Lett.* **2006**, *580*, 3823–3828.

(13) Hagiwara, Y.; Sugishima, M.; Takahashi, Y.; Fukuyama, K. *Proc. Natl. Acad. Sci. U.S.A.* **2006**, *103*, 27–32.

(14) Tu, S. L.; Rockwell, N. C.; Lagarias, J. C.; Fisher, A. J. *Biochemistry* **2007**, *46*, 1484–1494.

(15) Mayer, J. M. *Annu. Rev. Phys. Chem.* **2004**, *55*, 363–390.

(16) Un, S.; Dorlet, P.; Rutherford, A. W. *Appl. Magn. Reson.* **2001**, *21*, 341–361.

(17) Bennati, M.; Prisner, T. F. *Rep. Prog. Phys.* **2005**, *68*, 411–448.

(18) Smith, P. K.; Krohn, R. I.; Hemanson, G. T.; Mallia, A. K.; Gartner, F. H.; Provenzano, M. D.; Fujimoto, E. K.; Goeke, N. M.; Olsen, B. J.; Klenk, D. C. *Anal. Biochem.* **1985**, *150*, 76–85.

(19) Schluchter, W. M., Pennsylvania State University, 1994.

(20) McDonagh, A. F.; Palma, L. A. *Biochem. J.* **1980**, *189*, 193–208.

$P2_12_12$), with four sites per unit cell. The long, medium, and short edge of the crystal correspond to the crystallographic axes a, c, and b, respectively.

Frozen Solutions. Ferredoxin-reduced PcyA radical complexes were generated under anaerobic conditions. A volume of 1 mL of 200−300 mM substrate-bound protein was mixed with 10 μM bovine serum albumin, 50 μM Fd, 0.025 U/mL ferredoxin:NADP$^+$ oxidoreductase, and 10-fold excess of reduced NADPH. After 20 min, the reaction mixture was transferred to EPR sample holders and flash-frozen in liquid nitrogen. To generate dithionite-reduced PcyA-bound bilin radicals in frozen solutions, 200 μL of 3 mg/mL substrate-bound PcyA solution (20 mM TES, pH 8, 25% glycerol), plus an oxygen scavenging system (100 mM glucose, 50 U/mL glucose oxidase and 50 U/mL catalase) were mixed with 2.5 μL of 0.6 M sodium dithionite in the dark at room temperature in EPR sample containers and flash-frozen in liquid nitrogen after about 10 s incubation.

EPR Measurements. Continuous-wave EPR spectra (406 GHz) were obtained at the National High Magnetic Field Laboratory (NHMFL) in Tallahassee, FL, using a homodyne transmission-mode spectrometer,[21] at a microwave frequency of 406.4000(4) GHz ($g \approx 2.00$ around 14.52 T), a temperature of 45 K, and a peak-to-peak modulation amplitude of 0.1 mT at 50 kHz. Single-crystal measurements (130 GHz) were performed at the CalEPR center at the University of California Davis, at 45 K and 129.9966(4) GHz (in the D band) on a home-built pulse spectrometer with a microwave bridge similar to others described earlier,[22−24] equipped with a TE$_{011}$ cylindrical resonator and an 8 T cryogen-free magnet (Cryogenic Ltd., London). For the field sweeps, two-pulse echo detection with pulse lengths 50 and 100 ns, a τ value of 250 ns, 10 ms repetition times, and 20 accumulated echoes was used. The sample was rotated around the axis of the sample tube with a goniometer that covers a range of 200°. The accuracy of the angle rotations was about 0.1°. Spectra at 9.7 GHz were measured at 45 K on an ECS106 spectrometer (Bruker Biospin, Billerica MA), using 10 mW microwave power and 100 kHz modulation with 0.1 mT peak-to-peak amplitude.

Field Calibration. The magnetic field axes for the EPR measurements at 130 and at 406 GHz were calibrated using MgO with a Mn^{2+} impurity (95+% fused MgO, Aldrich) as internal standard.[25] The g and A values for Mn^{2+} were determined by least-squares fitting 9.7, 130, and 406 GHz spectra of the standard measured together with LiF:Li with known $g = 2.002293(2)$ as an internal reference,[26] yielding the g value $g = 2.00100(5)$, and the Mn^{2+} hyperfine coupling constant $A = -243.6(5)$ MHz. The value of the cubic parameter $a = 56$ MHz was taken from the literature.[27] For each sample, two spectra were acquired, one with the MgO: Mn^{2+} standard in the sample container and one without. The field axis in the first spectrum was calibrated by fitting a linear sweep to the known resonance fields of the Mn^{2+} transitions. The field axis for the second spectrum was obtained from the first by aligning the two radical spectra. The uncertainty in the field axis values results from the width of the Mn^{2+} lines of about 0.4 mT, translating to a g-value uncertainty of about 0.00005.

EPR Data Analysis. All EPR spectra from crystals and frozen solutions were simulated assuming a single unpaired electron (spin
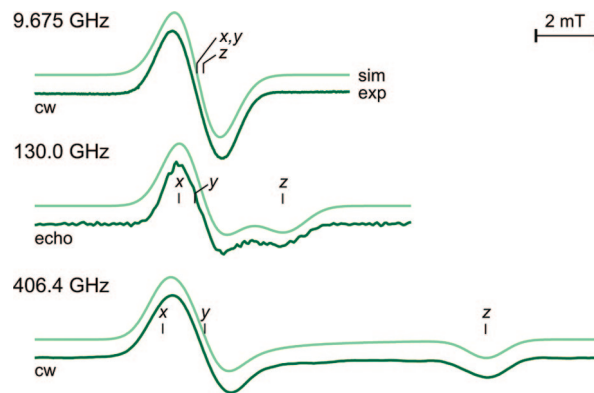
Figure 2. Experimental and simulated EPR spectra at 45 K of the frozen solutions of the reduced *Synechocystis* D105N·BV PcyA at three spectrometer frequencies. cw, cw field sweep; echo, derivative of echo-detected field sweep. x, y, and z indicate the positions corresponding to the principal g values. All spectra are centered at magnetic fields corresponding to $g \approx 2.003$.

1/2) with a general symmetric g tensor, $\mathbf{g}$. An isotropic Gaussian line broadening was included to model the broadening due to unresolved hyperfine splittings. The resonance field B for a given orientation of the magnetic field $\mathbf{n}$ relative to the crystal is given by $B = h\nu_{mw}/\mu_B g_{eff}$ with $g_{eff} = |\mathbf{n}^T\mathbf{g}|$, where h is the Planck constant, ν_{mw} is the spectrometer frequency, μ_B is the Bohr magneton, and g_{eff} is the effective g value for that orientation. The EPR spectrum of the orthorhombic crystal is the sum of the EPR subspectra arising from the four differently oriented but otherwise identical sites in the unit cell. For orientations where the applied magnetic field is oriented along one of the crystal axes a, b, or c, all four sites are magnetically equivalent and give identical resonance fields, so that only one EPR peak appears. If the field is in one of the crystal planes bc, ac, or ab, but not parallel to any crystal axis, the sites are pairwise magnetically equivalent, and two peaks result. For a general skew orientation not collinear with any crystal plane, the four sites are magnetically distinct, and four generally noncoincident peaks are found. All spectral simulations and least-squares optimizations (using the Nelder−Mead simplex algorithm) were performed using Matlab 7.3 (The MathWorks Inc., Natick, MA) and EasySpin 3.0.[28]

Quantum Chemical Calculations. Geometry optimizations in vacuo were performed with Gaussian 03 revision D.01 (Gaussian Inc., Wallingford CT) using density-functional theory (DFT) at the unrestricted B3LYP/3-21G* level. All g tensors were computed with Orca 2.6.35 (F. Neese, University of Bonn, Germany) using DFT in its coupled-perturbed Kohn−Sham formulation at the unrestricted BP86/SV(P) level.[29] For comparison with experimental g tensors, the asymmetric g matrices $\mathbf{g}_{as}$ obtained from the software were symmetrized[30] to yield the symmetric tensor $\mathbf{g} = (\mathbf{g}_{as}\mathbf{g}_{as}^T)^{1/2}$.

Results

Figure 2 shows the experimental and simulated EPR spectra of frozen solutions of the reduced substrate-bound D105N mutant of *Synechocystis* PcyA at three spectrometer frequencies. The anisotropy of the g tensor, not visible at 9.7 GHz, becomes partially resolved at 130 GHz. Only in the 406 GHz spectrum are the two limiting features of the spectrum (xy and z) completely separated. However, there are no resolved hyperfine splittings. The spectral broadening does not increase noticeably from 9.7 to 406 GHz. The broadening is thus due to unresolved

(21) Hassan, A. K.; Pardi, L. A.; Krzystek, J.; Sienkiewicz, A.; Goy, P.; Rohrer, M.; Brunel, L. C. *J. Magn. Reson.* **2000**, *142*, 300–312.
(22) Stich, T. A.; Lahiri, S.; Yeagle, G.; Dicus, M.; Brynda, M.; Gunn, A.; Aznar, C.; DeRose, V. J.; Britt, R. D. *Appl. Magn. Reson.* **2007**, *31*, 321–341.
(23) Lakshmi, K. V.; Reifler, M. J.; Brudvig, G. W.; Poluektov, O. G.; Wagner, A. M.; Thurnauer, M. C. *J. Phys. Chem. B* **2000**, *104*, 10445–10448.
(24) Mansoorabadi, S. O.; Seravalli, J.; Furdui, C.; Krymov, V.; Gerfen, G. J.; Begley, T. P.; Melnick, J.; Ragsdale, S. W.; Reed, G. H. *Biochemistry* **2006**, *45*, 7122–7131.
(25) Burghaus, O.; Rohrer, M.; Götzinger, T.; Plato, M.; Möbius, K. *Meas. Sci. Technol.* **1992**, *3*, 765–774.
(26) Stesmans, A.; Van Gorp, G. *Phys. Lett. A* **1989**, *139*, 95–98.
(27) Low, W. *Phys. Rev.* **1957**, *105*, 793–800.

(28) Stoll, S.; Schweiger, A. *J. Magn. Reson.* **2006**, *178*, 42–55.
(29) Neese, F. *J. Chem. Phys.* **2001**, *115*, 11080–11096.
(30) Törring, J. T.; Un, S.; Knüpling, M.; Plato, M.; Möbius, K. *J. Chem. Phys.* **1997**, *107*, 3905–3913.
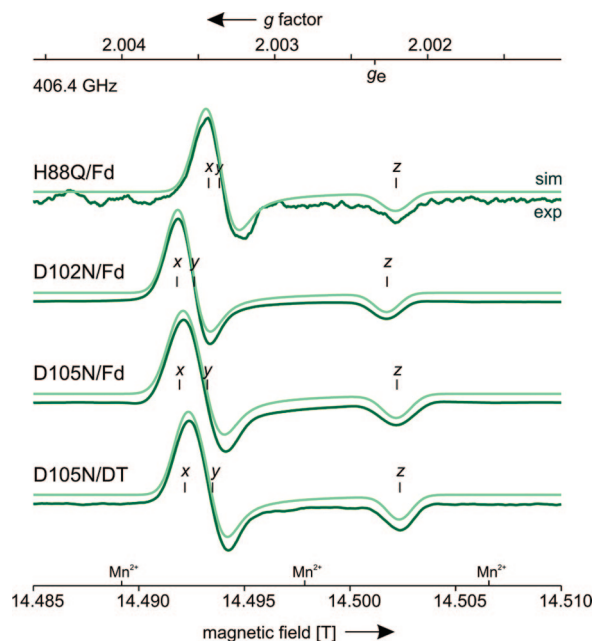
Figure 3. cw EPR spectra (406.4 GHz) of frozen solutions of the bound reduced BV substrate radical in PcyA mutants. g_e indicates the free-electron g factor 2.002319. Mn^{2+} indicates the position of three low-field lines of $MgO:Mn^{2+}$. The field positions corresponding to the three principal directions of the g tensor are indicated by x, y, and z.

hyperfine splittings alone, and there is no identifiable site-to-site variation in the g tensor principal values (g-strain).

The measured 406 GHz cw EPR spectra of frozen solutions of *Synechocystis* H88Q, *Nostoc* D102N and *Synechocystis* D105N mutants of PcyA are shown in Figure 3. The latter two possess mutations of the same residue, since residue 102 in *Nostoc* corresponds to 105 in *Synechocystis*. The lower signal-to-noise ratio of the spectrum of H88Q compared to those of the D102N and D105N mutants indicates that radical production is less efficient in H88Q, as was previously observed.[11] The simulated least-squares fitted spectra, also shown in the figure, agree very well with the experimental ones. Clearly, there is only one distinguishable spectroscopic species in each of the spectra. The g tensor principal values obtained from the least-squares fitting are listed in Table 1.

Echo-detected EPR spectra (130 GHz) of D105N·BV crystals were acquired in order to determine the orientation of the g tensor with respect to the crystal frame. The crystals were oriented in the sample tube such that for each, a crystallographic plane (ab, bc, and ac) was approximately parallel to the magnetic field vector. The angular increments in the crystal rotations were 10° for the ab plane and 5° for the other planes. The resulting rotation-dependent spectra are shown in Figure 4.

The usual procedure to analyze crystal rotation EPR data consists of picking the positions of all distinguishable peak maxima from the spectra and fitting a model to the resulting "road map" (a plot of rotation angle versus resonance positions).[31] In our case, the resonances from the four differently oriented sites in the crystal overlap and could not be resolved, so that the only viable way of analysis consisted of least-squares fitting directly to all the spectra simultaneously. Due to the small size of the crystals, perfect alignment of the crystal axes with the axis of the sample tube was not possible. To account for

this, the small misalignments were left variable in the least-squares optimization, so that a total of 16 parameters were fitted to 102 spectra: the three principal values and three Euler tilt angles of the g tensor, the line width of the isotropic Gaussian broadening, and the three crystal alignments with three Euler angles each. The fitting gave a set of four g tensors (g_1, g_2, g_3, g_4), one for each magnetically distinct site in the crystal. These g tensors have identical principal values but different orientations (different signs of the off-diagonal elements). The principal values are shown in Table 1, the full g tensors and their symmetry relations are given in the Supporting Information, Tables S3 and S4. The coordinates in the abc crystal coordinate frame of the principal axes of g_1 are listed in Table 2. The principal axes of the other three tensors, g_2, g_3, and g_4, are obtained by rotating the principal axes of g_1 through 180° about the b, c, and a axis, respectively. The principal axis z_1 corresponding to the smallest g value g_z is almost parallel to the c axis of the crystal frame ($\text{acos}(+0.9527) = 17.7°$).

If the three data sets had been obtained in exactly the three crystal planes, a second set of four g tensors, with principal values and orientations differing from the first set, would be expected to fit the experimental data equally well. This ambiguity can be resolved by measuring an EPR rotation pattern in a tilted plane and including it in the data analysis.[31,32] In our case, the small misalignments of the crystal meant that the ambiguity did not arise—any g tensor set corresponding to different g values and principal axes orientations had significantly larger fitting errors. Also, the g values of these additional sets are not consistent with those obtained from the frozen solution spectra (Table 1).

Discussion

Only one BV radical species is visible in the EPR spectra of Figures 2, 3, and 4. This confirms that the BV substrate is specifically targeted by both reductants (DT and Fd), without any collateral damage to potentially redox-active moieties such as Tyr residues that would yield significantly different EPR spectra. It is known that the reduction with dithionite proceeds via $SO_2^{•-}$ radicals,[33,34] which have principal g values of 2.0057(5), 2.012(3), and 2.002(2). There is no detectable sign of this radical species in the EPR spectra.

The line broadening is essentially the same in frozen solutions and crystals. The absence of g-strain deduced from the multi-frequency comparison in Figure 1 implies a high structural homogeneity of the bilin radical not only in the crystals, but also in frozen solutions of the protein. This has been observed before in protein-enclosed tetrapyrrole radicals.[35] However, tetrapyrrole radicals exposed to solvents can be strongly disordered and give rise to substantially broadened high-field spectra.[36] The hyperfine broadening of the spectrum of a fully deuterated BV radical would be smaller than the one observed here, and it should be possible to detect g-strain, if present. Such measurements are beyond the scope of the present study.

The g values from the frozen solutions of D105N·BV reduced with DT and Fd are identical within experimental error (see

(31) Isaacson, R. A.; Lendzian, F.; Abresch, E. C.; Lubitz, W.; Feher, G. *Biophys. J.* **1995**, *69*, 311–322.

(32) Schonland, D. S. *Proc. Phys. Soc. London* **1959**, *73*, 788–792.
(33) Lambeth, D. O.; Palmer, G. *J. Biol. Chem.* **1973**, *248*, 6095–6103.
(34) Reuveni, A.; Luz, Z.; Silver, B. L. *J. Chem. Phys.* **1970**, *53*, 4619.
(35) Bratt, P. J.; Heathcote, P.; Hassan, A.; van Tol, J.; Brunel, L. C.; Schrier, J.; Angerhofer, A. *Chem. Phys.* **2003**, *294*, 277–284.
(36) Bratt, P. J.; Poluektov, O. G.; Thurnauer, M. C.; Krzystek, J.; Brunel, L. C.; Schrier, J.; Hsiao, Y. W.; Zerner, M.; Angerhofer, A. *J. Phys. Chem. B* **2000**, *104*, 6973–6977.

Table 1. g Principal Values for Various BV Radicals in Semi-reduced PcyA·BV[a]

mutant		g_x	g_y	g_z	$g_x - g_z$	$(g_x - g_y)/(g_x - g_z)$	lw [mT]
Syn D105N/DT	fsl 406 GHz	2.00359(5)	2.00341(5)	2.00218(5)	0.00141(3)	0.13(4)	1.38(3)
Syn D105N/Fd	fsl 406 GHz	2.00362(5)	2.00344(5)	2.00220(5)	0.00142(3)	0.13(4)	1.57(3)
Nos D102N/Fd	fsl 406 GHz	2.00364(5)	2.00353(5)	2.00227(5)	0.00137(3)	0.08(4)	1.40(3)
Syn H88QN/Fd	fsl 406 GHz	2.00343(5)	2.00336(5)	2.00220(5)	0.00123(3)	0.06(4)	1.55(3)
Syn D105N/DT	xtl 130 GHz	2.00367(8)	2.00348(8)	2.00224(8)	0.00143(6)	0.13(4)	1.47(6)

[a] Syn, *Synechocystis*; Nos, *Nostoc*; DT, dithionite; Fd, ferredoxin; fsl, frozen solution; xtl, crystal; lw, Gaussian full width at half-maximum.
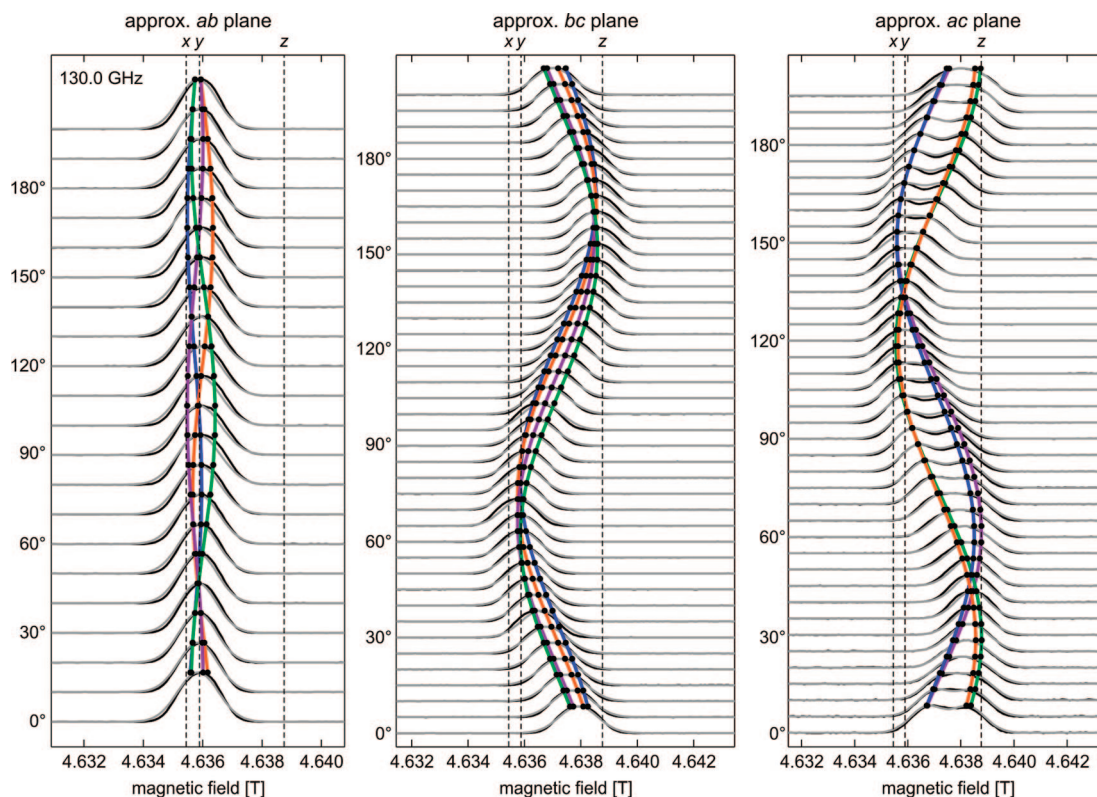

Figure 4. Two-pulse echo-detected EPR spectra of D105N·BV crystals soaked in DT, at 45 K and 130.0 GHz, for three different rotation planes. Black, experimental spectra; gray, simulations. Color: Resonance positions for the four sites as a function of rotation angle.

Table 2. Coordinates of the Principal Axes of g_1 in the *abc* Crystal Frame As Obtained from the D105N/DT Crystal Data Shown in Figure 4[a]

	x_1	y_1	z_1
a	+0.8373	−0.4709	−0.2777
b	+0.5172	+0.8469	+0.1237
c	+0.1770	−0.2421	+0.9527

[a] The estimated uncertainties in the orientations of the principal axes are 15° for x_1 and y_1 and 5° for z_1.

Table 1). Hence, the two reducing agents produce radical intermediates that are structurally indistinguishable in and around the region of unpaired spin density (BV and the surrounding amino acid residues). The g values for the D105N radical obtained from the 130 GHz crystal spectra and from the 406 GHz measurements on frozen solutions are almost identical, adding to the confidence in the accuracy of the measured g values at both frequencies. The g tensors of *Nostoc* D102N/DT and *Synechocystis* D105N/DT are slightly different. This is not surprising, since the sequences of the two organisms show only about 59% identity and some residues within 5 Å of the bilin substrate are different. Minor differences in BV conformation induced by nonconserved residues in the binding pocket thus might account for the small g tensor difference.
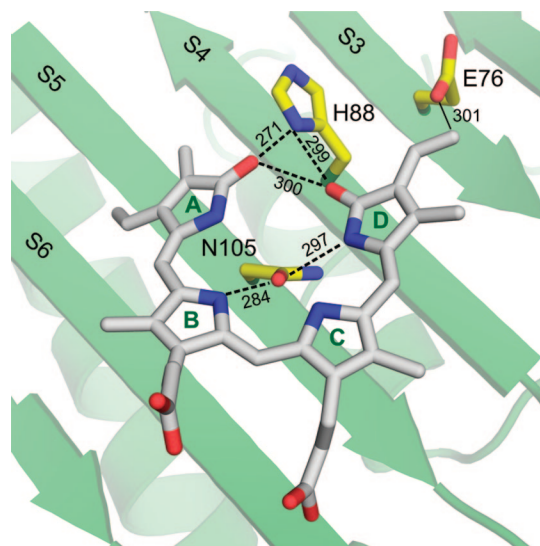
Figure 5. Structure of BV bound to PcyA D105N, including the three residues Glu76, His88, and Asn105. Distances are indicated in pm.

The g anisotropy of the BV radical in H88Q/Fd is measurably smaller than those of the other mutants. It is conceivable that

Table 3. Angles between the *z* Axes of the Four *g* Tensors and the Pyrrole Plane Normals of One BV Site

angle (deg)	A	B	C	D
z_1	2.8	28.5	27.5	4.4
z_2	14.4	42.5	37.1	17.5
z_3	32.8	56.1	62.6	39.6
z_4	29.5	45.6	56.6	35.6

the H88Q BV radical possesses a protonation state structurally distinct from that of D105N, especially since the His-to-Gln mutation eliminates a likely proton donor to the BV substrate. The small changes in the *g* principal values could also be attributed to different substrate environments due to indirect structural effects of the two mutated residues.

The principal *g* values of the BV radicals as listed in Table 1 all have a very small anisotropy of $g_x - g_z \approx 0.0014$, with only a hint of rhombicity, $(g_x - g_y)/(g_x - g_z) \approx 0.1$, that cannot be fully resolved at the highest field employed in this study, 14.5 T at 406 GHz. Numerical simulations show that even at the highest fields currently available (23.9 T, 670 GHz), the spectral features due to g_x and g_y would not be separated completely. Preliminary 130 GHz spectra of the radical intermediate in wild-type PcyA (not shown) reveal a *g* tensor similar to those of the mutants.

The shift of the principal *g* values from the free-electron value $g_e = 2.002319$ in an organic π radical depends on two principal factors: the number of heteroatoms (N and O) and the size of the π system.[30,37,38] The more heteroatoms there are, the larger the anisotropy, as each atom contributes to the *g* shift proportional to its spin–orbit coupling constant (C, 29 cm^{-1}; N, 76 cm^{-1}; O, 151 cm^{-1}).[39] The size of the π system affects the *g* shift through the ground-state and excited-state spin populations at the heteroatoms. The less spin there is at the heteroatoms, the smaller the *g* shift. All three principal *g* values of the BV radical deviate very little from g_e, which indicates that the unpaired electron is either confined to a relatively localized π system with C atoms only (e.g., the *g* values of a glycyl radical[40] are 2.0042, 2.0033, and 2.0023), or spread over a large delocalized π system containing N or/and O.

The line broadening of about 1.5 mT seen in all spectra is likely due to unresolved hyperfine splittings only, since it is field-independent. The size of the broadening and the lack of resolved hyperfine structure indicate that there are many small hyperfine couplings, none of them being sufficiently larger than the others to be resolved. In a localized radical, large ^{1}H hyperfine splittings would be expected, e.g., up to 2.8 mT in a glycyl radical.[41] Consequently, the unpaired electron appears delocalized over the entire BV molecule, rather than localized on one or a few C atoms. This is also supported by DFT, as discussed later. In preliminary ESEEM data (not shown), hyperfine couplings from multiple ^{14}N nuclei are detectable, further confirming a substrate radical with delocalized spin density.

In addition to characterizing the principal *g* values, we have also determined the orientation of the *g* tensor with respect to

(37) Stone, A. J. *Proc. R. Soc. London* **1963**, *271*, 424.
(38) Box, H. C. *Radiation Effects: ESR and ENDOR Analysis*; Academic Press: New York, 1977.
(39) Atherton, N. M. *Principles of Electron Spin Resonance*; Ellis Horwood: Chichester, 1993.
(40) Duboc-Toia, C.; Hassan, A. K.; Mulliez, E.; Ollagnier-de Choudens, S.; Fontecave, M.; Leutwein, C.; Heider, J. *J. Am. Chem. Soc.* **2003**, *125*, 38–39.
(41) Saxebøl, G.; Melø, T. B. T. H. *Radiat. Res.* **1972**, *51*, 31–44.
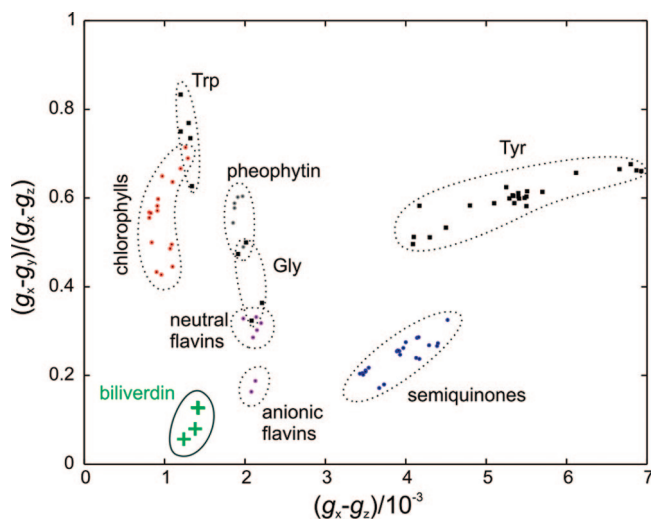
Figure 6. Comparative plot of experimental *g* tensors with principal values g_x, g_y, and g_z from various organic radicals occurring in biological systems.

the crystal. The X-ray crystal structure of the BV radical intermediate and the three essential residues Glu76, His88, and Asn105 is depicted in Figure 5. It is not possible to rigorously make a one-to-one assignment between the four *g* tensors obtained from the single-crystal EPR spectra and the four BV sites in the unit cell obtained from the X-ray crystal structure. However, in organic π radicals, it is known that *z*, the principal axis corresponding to the smallest *g* value g_z, is generally oriented perpendicular to the plane of the π system. The only known exception to this assertion is the primary donor cation radical of bacterial reaction centers, a bacteriochlorophyll dimer, where tilts out of the plane normal of up to 23° were found.[42,43] In monomeric π radicals however, no substantial tilts have been observed. We therefore expect the g_z axis to be approximately perpendicular to the π plane. In PcyA, the BV radical assumes a slightly nonplanar saddle conformation with the four pyrrole rings adopting slightly different orientations. The angle between the *z* orientations of the four *g* tensors and the normals of the four pyrrole planes of the reference site in the crystal data are listed in Table 3. Evidently, the z_1 axis of g_1 is almost aligned with the plane normals of rings A and D, and the frames of the other three *g* tensors are clearly further away from any plane normal than g_1. We therefore assign g_1 to the BV site. This assignment is supported by DFT computations (vide infra).

Figure 6 compares the principal values of the measured *g* tensors of BV to experimental values obtained by high-field EPR for a variety of organic π radicals from biological systems. In general, two *g* values, g_x and g_y, are larger than g_e and are indicative of the type of radical, whereas the third value, g_z, is very close to g_e, nearly identical in all these π radicals and thus of little diagnostic value. Since absolute *g* values can be measured less accurately than differences between *g* values due to the nature of the uncertainties in the field calibration, plotting the differences $g_x - g_z$ vs $(g_x - g_y)/(g_x - g_z)$ rather than g_x vs g_y in Figure 6 minimizes the impact of these field calibration uncertainty, which vary widely in the literature, if reported at all.

From this plot, it is evident that the EPR signature of the BV radical is very different from that of other types of radicals. In

(42) Klette, R.; Törring, J. T.; Plato, M.; Möbius, K.; Bonigk, B.; Lubitz, W. *J. Phys. Chem.* **1993**, *97*, 2015–2020.
(43) Huber, M.; Törring, J. T. *Chem. Phys.* **1995**, *194*, 379–385.

particular, tyrosyl radicals show a much larger *g* anisotropy, both in photosystem II (see refs 44 and 45 and references therein) and in ribonucleotide reductases.[46−49] The *g* tensor has been shown to be sensitive to the electrostatic environment of the radical and to hydrogen bonds to the phenoxy oxygen.[50] Semiquinone radicals also possess a larger *g* anisotropy,[31,51,52] and their *g* values exhibit a similar sensitivity to the environment.[53−55] The EPR spectra of both neutral and anionic flavin radicals,[56−60] as well as glycyl radicals,[40] are almost twice as wide as that of BV. By comparison, the *g* tensor of tryptophanyl radicals is more similar to BV in anisotropy, but much more rhombic.[61−63] While the *g* anisotropy of the BV radical is also similar to those of pheophytin and chlorophylls in photosystem II,[23,42,64−66] its *g* tensor is much less rhombic. Indeed, the *g* tensors of the BV radicals measured in this study are among the most axial reported so far for organic π radicals.[67]

To determine the protonation state of the BV radical responsible for the EPR spectrum, we computed the *g* tensors of many possible protonated radical species for the D105N mutant using DFT. DFT is known to predict *g* tensors of

organic radical quite accurately,[68] with a tendency to overestimate *g* shifts by up to 10%.[53] For various protonated species of the BV radical, positions of all hydrogens were optimized using the frozen heavy-atom geometry of BV obtained from the diffraction data of the dithionite-reduced crystal (Fisher et al., unpublished data). The three catalytic residues Glu76, His88, and Asn105 of PcyA were included in these calculations with the backbone subunit of each amino acid replaced by a hydrogen attached to the α-carbon. The inclusion of these amino acids side chains is important, since they are known to be essential in catalysis as proton donors.[10] All three residues are capable of hydrogen bonding to the protonated BV substrate and thus are critical for determining the locations of protons on BV. Additionally, their presence can influence the *g* tensor through electrostatic effects. To reduce the system to a computationally feasible size, we replaced the two propionate side groups on the B and C rings with methyl groups. The propionate groups are far from the active center and from the active center and from the π system, so their effect on the *g* tensor is small.

There are seven potential protonation sites in the reduced BV radical (see inset in Figure 7): the four pyrrole nitrogens denoted A, B, C, and D, the two carbonyl oxygens on the A and the D rings denoted α and δ, and the terminal carbon on the D-ring vinyl group denoted by v. Protonation at the A-ring vinyl is not taken into account, as it is known that it is targeted only in the second reaction (see Figure 1). For the neutral substrate, the bis-lactam forms of a native BV molecule would possess protons on three of the four nitrogen atoms, designated ABD or ACD in our shorthand notation., while the designations αBD and ABδ correspond to two possible monolactim species. On the basis of the proposed mechanism of PcyA, the reduced BV radical could possess up to two additional protons.[14] Therefore, possible structures for the BV radical intermediate include anion radicals (BV$^{\bullet-}$, three protons total, e.g., ABD$^{\bullet-}$), neutral protonated radicals (HBV$^{\bullet}$, four protons, e.g., ABD$\delta^{\bullet}$) and doubly protonated cation radicals (H$_2$BV$^{\bullet+}$, five protons, e.g., ABDδv$^{\bullet+}$). Divalent cation radicals H$_3$BV$^{\bullet2+}$ with a total of six protons are chemically unlikely. Indeed, BV dication radicals are not stable in the DFT ^{1}H geometry optimizations, as for example αABCD$\delta^{\bullet2+}$ sheds its α proton to the proximal imidazole nitrogen of His88. All geometrically possible single and double protonation states of the His88 imidazole ring were included. The side-chain carboxylate of Glu76 was assumed to be protonated except in the species with v-protonation. Anion radicals with v-protonation were not included in these analyses.

All the optimized structures yielded ground-state wave functions with spin densities completely delocalized over the entire π system of the molecule. After optimization, the *g* tensors were computed for the optimized structures, keeping all three amino acids residues. The DFT results are shown in Figure 7 (see Supporting Information, Table S5, for a list of all the *g* tensors principal values and Table S6 for the absolute energies). For protonated species without v-protonation, *g* tensors fall into three groups depending on the degree of protonation of the two carbonyl oxygens. When both oxygens are unprotonated, i.e., when BV is in a bis-lactam form, the *g* tensor anisotropy is rather large and similar to tyrosyl radicals, but strongly dependent on which nitrogens are protonated. Bis-lactam rhombicity is close to 0.5, slightly

(44) Un, S.; Tang, X. S.; Diner, B. A. *Biochemistry* **1996**, *35*, 679–684.
(45) Hofbauer, W.; Zouni, A.; Bittl, R.; Kern, J.; Orth, P.; Lendzian, F.; Fromme, P.; Witt, H. T.; Lubitz, W. *Proc. Natl. Acad. Sci. U.S.A.* **2001**, *98*, 6623–6628.
(46) Un, S.; Atta, M.; Fontecave, M.; Rutherford, A. W. *J. Am. Chem. Soc.* **1995**, *117*, 10713–10719.
(47) van Dam, P. J.; Willems, J. P.; Schmidt, P. P.; Pötsch, S.; Barra, A. L.; Hagen, W. R.; Hoffman, B. M.; Andersson, K. K.; Gräslund, A. *J. Am. Chem. Soc.* **1998**, *120*, 5080–5085.
(48) Högbom, M.; Galander, M.; Andersson, M.; Kolberg, M.; Hofbauer, W.; Lassmann, G.; Nordlund, P.; Lendzian, F. *Proc. Natl. Acad. Sci. U.S.A.* **2003**, *100*, 3209–3214.
(49) Galander, M.; Uppsten, M.; Uhlin, U.; Lendzian, F. *J. Biol. Chem.* **2006**, *281*, 31743–31752.
(50) Engström, M.; Himo, F.; Gräslund, A.; Minaev, B.; Vahtras, O.; Agren, H. *J. Phys. Chem. A* **2000**, *104*, 5149–5153.
(51) Burghaus, O.; Plato, M.; Rohrer, M.; Möbius, K.; Macmillan, F.; Lubitz, W. *J. Phys. Chem.* **1993**, *97*, 7639–7647.
(52) Kay, C. W. M.; Mennenga, B.; Gorisch, H.; Bittl, R. *J. Am. Chem. Soc.* **2005**, *127*, 7974–7975.
(53) Kaupp, M.; Remenyi, C.; Vaara, J.; Malkina, O. L.; Malkin, V. G. *J. Am. Chem. Soc.* **2002**, *124*, 2709–2722.
(54) Kacprzak, S.; Kaupp, M.; MacMillan, F. *J. Am. Chem. Soc.* **2006**, *128*, 5659–5671.
(55) Sinnecker, S.; Flores, M.; Lubitz, W. *Phys. Chem. Chem. Phys.* **2006**, *8*, 5659–5670.
(56) Kay, C. W. M.; Bittl, R.; Bacher, A.; Richter, G.; Weber, S. *J. Am. Chem. Soc.* **2005**, *127*, 10780–10781.
(57) Fuchs, M. R.; Schleicher, E.; Schnegg, A.; Kay, C. W. M.; Törring, J.; Bittl, R.; Bacher, A.; Richter, G.; Möbius, K.; Weber, S. *J. Phys. Chem. B* **2002**, *106*, 8885–8890.
(58) Barquera, B.; Morgan, J. E.; Lukoyanov, D.; Scholes, C. P.; Gennis, R. B.; Nilges, M. J. *J. Am. Chem. Soc.* **2003**, *125*, 265–275.
(59) Okafuji, A.; Schnegg, A.; Schleicher, E.; Möbius, K.; Weber, S. *J. Phys. Chem. B* **2008**, *112*, 3568–3574.
(60) Kay, C. W. M.; El Mkami, H.; Molla, G.; Pollegioni, L.; Ramsay, R. R. *J. Am. Chem. Soc.* **2007**, *129*, 16091–16097.
(61) Bleifuss, G.; Kolberg, M.; Pötsch, S.; Hofbauer, W.; Bittl, R.; Lubitz, W.; Gräslund, A.; Lassmann, G.; Lendzian, F. *Biochemistry* **2001**, *40*, 15362–15368.
(62) Miller, J. E.; Grădinaru, C.; Crane, B. R.; Di Bilio, A. J.; Wehbi, W. A.; Un, S.; Winkler, J. R.; Gray, H. B. *J. Am. Chem. Soc.* **2003**, *125*, 14220–14221.
(63) Pogni, R.; Baratto, M. C.; Teutloff, C.; Giansanti, S.; Ruiz-Duenas, F. J.; Choinowski, T.; Piontek, K.; Martinez, A. T.; Lendzian, F.; Basosi, R. *J. Biol. Chem.* **2006**, *281*, 9517–9526.
(64) Bratt, P. J.; Rohrer, M.; Krzystek, J.; Evans, M. C. W.; Brunel, L. C.; Angerhofer, A. *J. Phys. Chem. B* **1997**, *101*, 9686–9689.
(65) Dorlet, P.; Xiong, L.; Sayre, R. T.; Un, S. *J. Biol. Chem.* **2001**, *276*, 22313–22316.
(66) Petrenko, A.; Maniero, A. L.; van Tol, J.; MacMillan, F.; Li, Y. J.; Redding, K. *Biochemistry* **2004**, *43*, 1781–1786.
(67) Konovalova, T. A.; Krzystek, J.; Bratt, P. J.; van Tol, J.; Brunel, L.-C.; Kispert, L. D. *J. Phys. Chem. B* **1999**, *103*, 5782–5786.

(68) Benisvy, L.; Bittl, R.; Bothe, E.; Garner, C. D.; McMaster, J.; Ross, S.; Teutloff, C.; Neese, F. *Angew. Chem., Int. Ed.* **2005**, *44*, 5314–5317.
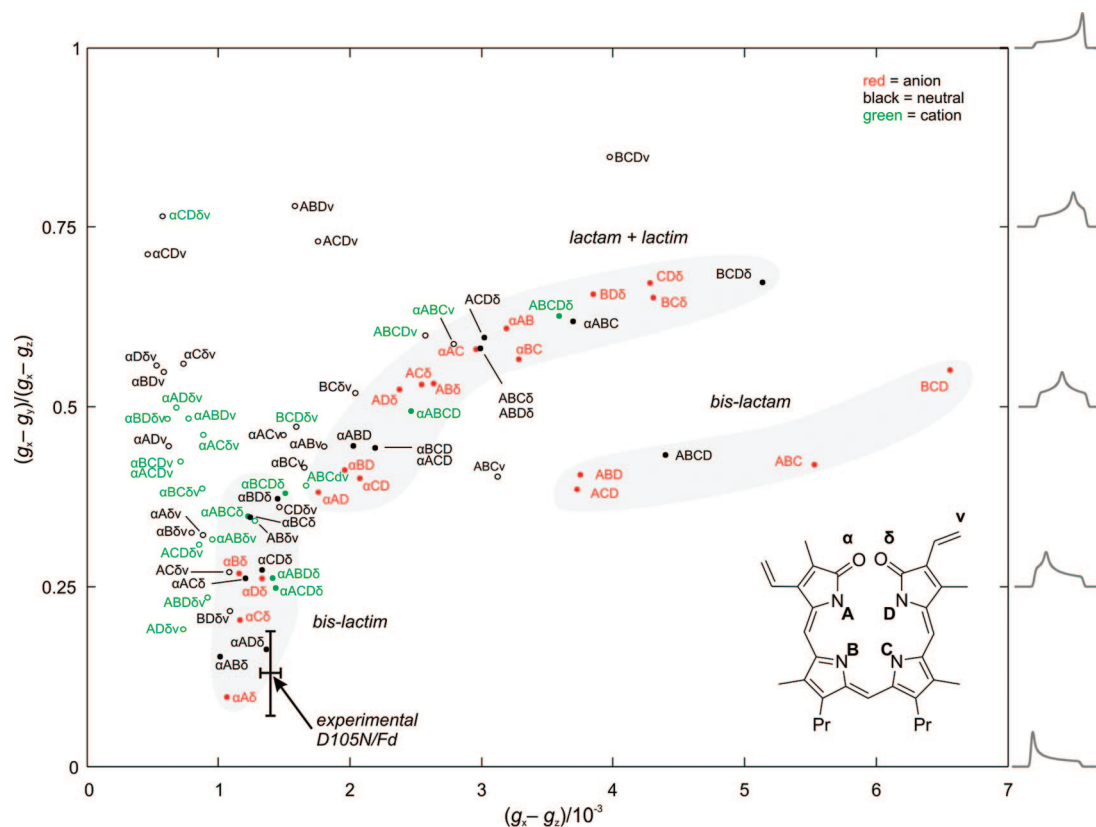
Figure 7. DFT predictions of *g* tensors of various protonation species of the BV radical in D105N PcyA.

smaller than that found in tyrosyl radicals. When one of two carbonyl oxygens is protonated to yield monolactim species, *g*-tensor anisotropies, and rhombicity values both spread over a larger range. Like the bis-lactam radicals, monolactim/monolactam radical anisotropies are also sensitive to the protonation state of the nitrogens. The third class of BV radicals adopt a bis-lactim form where both carbonyl oxygens are protonated (αδ). The *g* anisotropy of these species is much smaller than in the two other groups, since the contributions to the *g* shift from both carbonyl oxygens shrink. All nitrogens and even some carbons contribute to the total g shift of these species. A similar drastic decrease in g_x and g_y upon O protonation has recently been observed in semiquinone moieties in humic acids.[69] Interestingly, while the exact protonation state of the pyrrole nitrogens does not affect the *g* anisotropy of the bis-lactims, this strongly changes the rhombicity of the *g* tensor via the g_y value. The reason for this is not entirely clear, since one expects that N protonations would change both g_x and g_y in a roughly similar fashion. The 35 BV radical protonation species that possess a proton on the D-vinyl group give *g* tensors that are more difficult to rationalize. There is no obvious correlation of the anisotropy or the rhombicity to the structure of these protonation states. Their anisotropy values tend to be smaller than those of species with nonprotonated D-ring vinyl groups.

In all protonation states shown in the figure, His88 is assumed protonated at the imidazole nitrogen distal to BV. For the bis-lactims and the monolactim/monolactam forms of BV, there are other possible His88 protonations, either of the nitrogen proximal to BV (shorthand h) or of both imidazole nitrogens

(69) Witwicki, M.; Jaszewski, A. R.; Jezierska, J.; Jerzykiewicz, M.; Jezierski, A. *Chem. Phys. Lett.* **2008**, *462*, 300–306.

(shorthand x). They lead to changes in the g values but stay consistent within the groupings in Figure 7 (see Supporting Information, Table S5).

On the basis of the data shown in Figure 7, the measured *g* tensor of D105N/DT (and all the other D105N samples) proves most similar with those calculated for the bis-lactims (αδ) and some v-protonated species (δv). We therefore conclude that the D-ring oxygen and either the A-ring oxygen or the terminal D-ring vinyl carbon are protonated upon BV reduction. The total charge of the radical cannot be inferred from the DFT predictions. Although there are two anion radicals, αAδ•⁻ and αCδ•⁻, with *g* tensors close to the experimental ones, anions are unlikely except as transient species: the nonbound substrate has three protonated nitrogens, and there is no reason to expect two proton abstractions from the nitrogens during the reaction. Neutral and cation radicals are much more likely. The neutral radical αADδ• comes closest to the experimental *g* value, whereas among the radical cations αABDδ•⁺ and αACDδ•⁺ are potential candidates. Among the species protonated on the terminal vinyl carbon, BDδv•, ACδv•, and ABDδv• are the best candidates, although the *g* tensors of these δv species deviate more from the measured ones than those of the αδ species. Also, the large isotropic hyperfine interaction expected for the protons of the terminal CH₃ group in the v protonation states should lead to resolved hyperfine splittings, which are not discernible in our measured spectra.

The structure of αABDδ•⁺ and the SOMO of its ground-state wave function are shown in Figure 8. The proton on the A-ring oxygen is hydrogen-bonded to His88, while the proton on the D-ring oxygen is directed toward the A-ring oxygen. An alternative structure of αABDδ•⁺, where both the A-ring and the D-ring protons hydrogen-bond to His88,
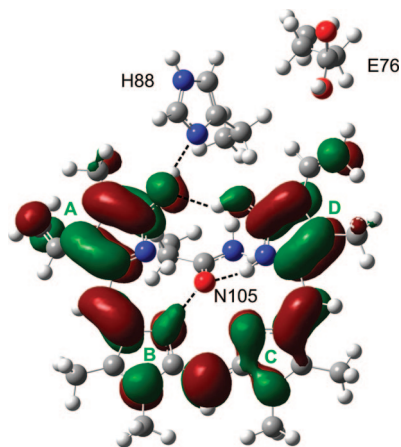
Figure 8. BV radical cation $\alpha ABD\delta^{\bullet+}$, including amino acid residues His88, Asn105, and Glu76. SOMO surface (isovalue 0.02).

is about 7 kJ/mol higher in energy. As in all PcyA structures known so far,[12−14] BV assumes a saddle conformation, where the B and D rings are slanted inward and downward toward Asp/Asn105, allowing the protons of the B and D ring pyrrole nitrogens to hydrogen-bond to the carbonyl oxygen of residue 105. In contrast, the A and C rings are pointing upward toward Asn219 (not shown), avoiding steric crowding in the ring plane.

The predicted $\alpha\delta$-structure of the radical strongly supports the detailed reaction mechanism proposed recently for the wild type.[14] BV (e.g., in its ABD form) undergoes protonation or internal proton transfer during or after binding to wild-type PcyA, yielding, e.g., $ABD\delta^+$ or $AB\delta$. This raises the reduction potential enough so that the first electron is transferred from Fd to BV, resulting in $ABD\delta^{\bullet}$ or $AB\delta^{\bullet-}$. These states are a neutral or anionic radical, but their predicted g tensors are inconsistent with the measured ones, as only one of the two carbonyl oxygens is protonated. Thus, the reduction is quickly followed (or accompanied) by a second protonation to the other carbonyl oxygen giving $\alpha ABD\delta^{\bullet+}$ or $\alpha AB\delta^{\bullet}$. These protonated species are consistent with DFT and the high-field EPR observations. An anion radical $\alpha B\delta^{\bullet-}$, obtained from $AB\delta^{\bullet-}$ by lactam−lactim tautomerization is also a formal possibility. From DFT, we cannot completely exclude a radical with δv protonation. Such a radical could be produced from $\alpha ABD\delta^{\bullet+}$ or $\alpha AB\delta^{\bullet}$ via an internal rearrangement of the O-protons, e.g., $\alpha ABD\delta^{\bullet+} \rightarrow \alpha ABDv^{\bullet+} \rightarrow ABD\delta v^{\bullet+}$, or via direct protonation of the terminal D-ring vinyl carbon by the protonated side group of the nearby Glu76.

Two key questions remain for future studies. First, how is BV protonated to HBV^+ in the mutant D105N which lacks the potential proton donor Asp105 found in wild-type? While the D105N mutation does not completely destroy activity, it slows down[11] the primary electron transfer by a factor of about 10. Therefore, we propose that initial protonation in this mutant must come either from a proton channel via His88 or from a close-by water molecule. Alternatively, BV protonation could even be derived from the A or D ring nitrogens via a lactam−lactim tautomerization equilibrium, yielding a neutral singly O-protonated BV. The latter pathway would also be consistent with the fact that the UV/vis spectrum of bound BV in D105N lacks the absorption shoulder at 750 nm observed for bound BV in wild-type PcyA.[11] Second, why is the radical, once generated, more stable compared to the radical in the wild type?[11] The reaction from the $\alpha\delta$ radical to the eventual

diamagnetic intermediate DHBV must proceed either stepwise via an ET followed by a PT or by a concerted PCET. The first possibility would be reasonable if the redox potential of the radical intermediate in the mutant is significantly lower than in the wild type. This could only be explained if the first proton on O comes from an internal lactam−lactim rearrangement. The second pathway seems more probable, as it might be slowed down by the absence of the fast proton shuttle via Asp105. With Asn105 instead, the proton must find its way to the substrate either via a close-by bound water molecule, via a solvent-connected proton channel ending in His88, or via lactam/lactim tautomerization. The decreased rates of radical generation and of its decay indicate that a slow protonation rate could indeed be the bottleneck in the mutant. Asp105 appears not only important for initial protonation during substrate binding but also for delivering the two constitutive protons for the reduction of the D-ring vinyl group. It is possible that both electron transfers are concerted PCETs rather than sequential electron and proton transfers.

Although the high-field EPR and DFT results strongly suggest the presence of a doubly protonated BV radical of type $\alpha\delta$ (or δv), there remain ambiguities as to the total charge and exact protonation geometry of the radical. These can be addressed by advanced pulse EPR experiments. [14]N electron-spin−echo envelope modulation (ESEEM) studies are under way to determine the spin populations and the electric field gradients at the four pyrrole nitrogen atoms. From these data, the protonation states of the nitrogens are deducible. [1]H electron−nuclear double resonance (ENDOR) at high field combined with deuterium exchange will allow the exact position of the protons present in the radical to be determined. A fully deuterated BV substrate will also help to determine the g tensor more accurately. Although we have included three catalytically important residues in the DFT computations, it is possible that the entire binding pocket must be included to attain reliable g tensor predictions.

We realize that the mechanistic conclusions above are based on data from the mutant D105N and they have to be reevaluated for the wild type. The production of the radical intermediate in wild type PcyA is more difficult, as it requires rapid freeze-quenching. It is the subject of future studies.

Conclusions

The combination of advanced high-field EPR and DFT calculations allowed us to extract an unexpected amount of structural information from a radical that gives only one single resonance line at conventional X-band EPR frequencies: The radical intermediate generated by reduction of the D105N mutant of substrate-bound PcyA is a biliverdin radical with a high-field EPR spectrum revealing a narrow, almost axial g tensor, with the unique axis perpendicular to the A and the D ring of the aromatic π electron system. The extremely small anisotropy of the g tensor indicates that the two carbonyl oxygens on the A and the D ring of the BV radical are protonated. DFT computations support this conclusion, as other protonated species without or with only one protonated oxygen are predicted to have g tensors that are significantly more anisotropic and more rhombic than the experimental ones. This finding confirms the suggested radical intermediates in a recently proposed reaction mechanism. The results presented in this work lay the ground for characterizing the transient radical intermediate in wild-type PcyA.

Supporting Information Available: Tables S1−S6. This material is available free of charge via the Internet at http://pubs.acs.org.

JA808573F